Pol. J. Environ. Stud. Vol. XX, No. X (XXXX), 1–11
DOI:*10.15244/pjoes/184150* ONLINE PUBLICATION DATE:

Original Research

Influence of TiO_2 Nanoparticles Synthesizing Techniques on Photocatalytic Degradation of Methylene Blue Dye"

Saleh M. Alluqmani[1], Asla A. AL-Zahrani[2, 3], Hana Mohammed Almarri[3, 4], Nadiyah M. Alabdallah[3, 5] *

[1]Department of Physics, Faculty of Applied Science, Umm Al-Qura University, Makkah 21955, Saudi Arabia
[2]Department of Chemistry, College of Science, Imam Abdulrahman Bin Faisal University, P.O. Box 1982, Dammam, 31441, Saudi Arabia
[3]Basic and Applied Scientific Research Center- College of Science -Imam Abdulrahman Bin Faisal Abdulrahman bin Faisal University, P.O. Box 1982, Dammam, 31441, Saudi Arabia
[4]Department of Physics, College of Science, Imam Abdulrahman Bin Faisal University, P.O. Box 1982, Dammam, 31441, Saudi Arabia
[5]Department of Biology, College of Science, Imam Abdulrahman Bin Faisal University, P.O. Box 1982, 31441, Dammam, Saudi Arabia

Received: 10 December 2023
Accepted: 15 February 2024

Abstract

Model photocatalysts composed of titanium dioxide (TiO_2) nanoparticles were prepared to assess the impact of different synthesis techniques on their photocatalytic activity towards methylene blue. TiO_2 nanoparticles were synthesized using three distinct methods: high-energy ball-milling (HEBM), sonication, and pulse laser ablation. The engineered photocatalysts exhibited varying morphology, crystallinity, and optical properties, as evidenced by scanning electron microscopy (SEM) and X-ray diffraction (XRD). The synthesis techniques notably resulted in different particle sizes, with mean sizes of 121.2 nm, 25.53 nm, and 22.38 nm, and corresponding crystallite sizes of 24.86 nm, 33.5 nm, and 34.4 nm for HEBM, sonication, and pulse laser ablation, respectively. All of the synthesized TiO2 nanoparticles displayed significantly enhanced photocatalytic activity under low-intensity UV light in comparison to the TiO_2 raw material. However, the choice of synthesis method had a substantial impact on photocatalytic performance. Specifically, TiO_2 prepared via ultrasonication and continuous ball milling exhibited the highest photocatalytic activity among the methods. The most rapid degradation rate (K = 0.0049 min^(-1)) was observed for TiO_2 produced through continuous ball milling and ultrasonication. These findings indicate that the synthesized TiO_2 nanoparticles hold potential for use as catalysts for degrading various types of organic pollutants.

Keywords: characterization, photocatalytic activity, photocatalyst synthesis, TiO_2 nanoparticles, water purification

*e-mail: nmalabdallah@iau.edu.sa

Introduction

One of the significant challenges posing a threat to clean water quality is the presence of organic dye pollutants. Water contaminated by these pollutants is detrimental to both human health and the environment. In light of the world's burgeoning population, the imperative for advanced wastewater treatment technologies has escalated into a critical global issue. Various approaches have been employed to address the issues associated with water pollution, aimed at mitigating the presence of organic dyes. These methods include filtration, chemical precipitation, adsorption, membrane processes, and advanced oxidation techniques. Nevertheless, the advanced oxidation process, as demonstrated by the photocatalysis model, stands out as a cost-effective and environmentally friendly means of breaking down harmful compounds found in wastewater and the surrounding environment [1, 2].

Hence, it is of high importance to optimize and engineer a developed catalyst for organic dye degradation as well as remediation methods. Metal oxide semiconductors are used as photocatalysts because of their intermediate energy bandgap. Among them, titanium dioxide (TiO_2) is the most utilized semiconductor in photocatalysis because of its abundance, chemical stability, non-toxicity, and adequate band edge [3]. A critical topic for scientists working in this area is to realize the physical, chemical, and biological properties and develop strategies for advanced nanocomposites fabricated by eco-friendly, scalable, and low-cost synthetic approaches. There are multiple distinct polymorphs of TiO_2 with varying characteristics. The three most prevalent ones are anatase, brookite, and rutile. Anatase and rutile For photocatalytic performance, TiO_2 is the most often employed polymorph and is recommended above amorphous nature. [4]. Therefore, the crystal nature of the TiO_2 structure highly affects the application performance. However, in application, TiO_2 has a high recombination rate of photogenerated carriers (electron-hole) pairs, low capacity of adsorption, and low thermal stability, which limits its intrinsic activity [5]. Thus, strategies that can be put into action to face these challenges include the modification of TiO_2 by altering its morphology, crystallinity, and optical behavior by adding dopants [6], applying temperature treatment [7], and using the photon induction method [8]. On the other hand, in this regard, the TiO_2 response to photoexcitation is limited by electron-hole pair recombination, so photocatalytic performance could be enhanced by the preparation method. Various forms of TiO_2 nanostructures can be synthesized using a variety of techniques [9-12], depending on the specific application. The morphological forms and crystallinity of TiO_2, and impurities content and defects produced from several synthetic techniques, have considerable effects. The dynamics of photogenerated carriers pairs are strongly influenced by surface morphology and crystal modification [12, 13]. It is believed that modified TiO_2 has an impact on the photogenerated carriers pairs mobility and potential separation.

To the best of our knowledge, few studies are specifically devoted to affecting the phase transformation of titania at room temperature and its impact on the photocatalytic performance [5]. Here we design, engineer, and evaluate simple model nanoparticles of TiO_2 with the aim of understanding the role of nanoparticles prepared using different technologies on the photocatalytic performance of TiO_2. Thus, bulk material is converted into small, nano-sized particles. We adopt widely used physical techniques such as high-energy ball-milling (HEBM), sonication, and laser ablation techniques to synthesize and modify TiO_2 nanoparticles. Special reflection is given to the size and morphology, crystallinity, and photocatalytic properties of TiO_2 and their relationship with photogenerated carriers pairs dynamics. Furthermore, we measure the photocatalytic activity of synthetic and modified TiO_2 nanoparticles to examine the degradation rate of the blue dye in water. Here, we aim to quantitatively measure the degradation rate of the blue dye in water, providing a tangible metric to gauge the effectiveness of the synthesized and modified nanoparticles. Through this, the study aspires not only to contribute valuable insights to the field of photocatalysis but also to pave the way for future advancements in the synthesis and application of photocatalytic materials.

Materials and Methods

Materials

Titanium dioxide nanoparticles (TiO_2 NPs) were produced through three widely recognized preparation methods, utilizing high-purity (99.8%) titanium dioxide (TiO_2).

High-Energy Ball-Milling

The milling process induces alterations in micron-sized materials. Various milling machines are employed in the synthesis of nanoparticles. While this method offers advantages such as ease of operation, cost-effectiveness, and suitability for large-scale production, it does come with limitations, including the challenge of producing ultrafine particles, which can be time-consuming [14]. The quality of the final product depends on several factors, including the type of mill, milling speed, temperature, time, atmosphere, and container [15].

High-energy ball-milling (HEBM) is a mechanical alloying process where a powder mixture placed in a ball mill undergoes high-energy collisions with the balls [16]. This technique is capable of producing fine, uniform dispersions of oxide particles not achievable through conventional powder metallurgy methods [17]. Mechanical milling reduces particle size through high-energy ball milling, wherein bulk powder is added to a container with heavy balls. High mechanical energy is applied to the bulk powder material via high-speed rotating balls, leading to particle size reduction [18].

A grinding device called a ball mill can be used to synthesize nanoparticles at low temperatures without any

Fig. 1. The Vibra Cell Ultrasonic (CV334) sonication machine use in this study.

requirement for input heating [19]. The reactants deform, fractionate, and weld throughout the milling process. By-product material is distributed in a soluble salt matrix and encases the generated nanoparticles. The by-product is then removed by washing the particles in an appropriate solvent and drying them for 12 hours at 105°C [20].

Preparation of TiO_2 Nanoparticles Using the Sonication Method

The raw TiO_2 was subjected to a sonication process for five hours using a UIP500 HDT probe sonicator, Vibra Cell Ultrasonic (CV334) from Hielscher Ultrasound Technology, Teltow, Germany, as illustrated in Fig. 1. The sonicator operated at approximately 100 W with a signal amplitude of around 80%. Initially, 5 grams of powder were dispersed in approximately 500 mL of deionized water within a beaker. Subsequently, the probe was submerged in the solution. Following the desired sonication period, the solution was subjected to drying at approximately 70°C to obtain powdered samples.

Preparation of TiO_2 Nanoparticles Pulse Laser Ablation

Pulsed laser ablation (PLA) is an appealing synthesis method due to its capacity for generating nanoparticles characterized by a narrow size distribution and minimal impurity content [21]. In the laser ablation process, laser irradiation is employed to reduce the particle size to the nanoscale. A solid target material is positioned beneath a thin layer and subsequently subjected to pulsed laser irradiation. The irradiation of the material with the laser causes the solid material to fragment into nanoparticles, which persist in the liquid surrounding the target, resulting in the creation of a colloidal solution [22]. The relative number of ablated atoms and resulting particles is determined by the laser pulse duration and energy [22]. In this experiment, two distinct models of Q-switched Nd: YAG pulsed lasers (PS- 2225, LOTIS TII Ltd., Minsk, Belarus) were used to produce TiO2 nanoparticles. The first model had a repetition rate of 10 Hz, a wavelength of 355 nm, and a pulse energy of 120 mJ. Using a 10 ns pulse width, TiO_2 nanoparticles have been generated. After positioning the TiO_2 target at the bottom of a glass vial holding 10 milliliters of deionized water, the target was ablation-treated for half an hour. The primary focal point of the laser beam was moved below the liquid's surface to avoid high fluence, which may potentially ablate the surface-air interface and stop liquid splashing. The PLA process concept is shown in Fig. 2.

Characterization Methods

Various techniques were employed to confirm the characterization of TiO_2 nanoparticles. In this study, the formulation of TiO_2 nanoparticles through different methods was assessed by measuring the UV-visible spectrum (UV–vis) using equipment from Shimazu in Kyoto, Japan. The UV–vis results of the prepared nanoparticles displayed an optical absorption peak, signifying efficient detection of surface plasmon resonance. Structural analysis of the powdered samples was conducted using scanning electron microscopy (SEM) with equipment from JEOL in Tokyo, Japan. The powder was sprayed onto a carbon strip that was connected to the sample container in order to prepare the samples for SEM, which were then assessed at room temperature. After being temporarily submerged

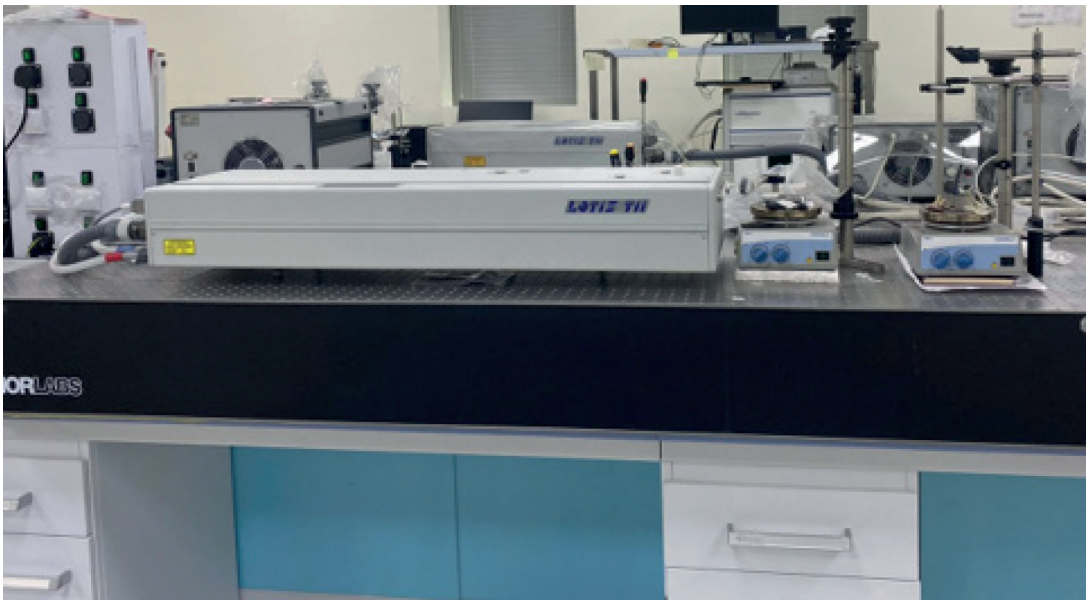

Fig. 2. The motorized XY stage's target is focused by a pulsed laser beam coupled to the mirror and lens in the laser ablation system.

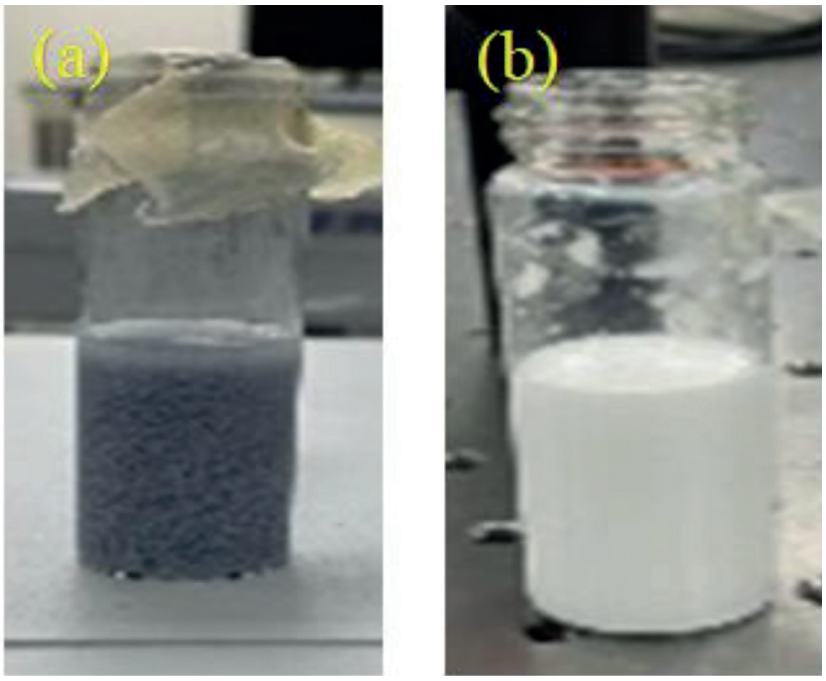

Fig. 3. TiO_2 suspended solution (a)before (b) after laser ablation.

in the sonicated powder sample, a copper grid with an approximate 400 mesh size from Sigma Aldrich in Saint Louis, MO, USA, was let to air dry at ambient temperature. The grid was placed on a sample holder and examined at 100 kV when it was still at room temperature after it had completely dried. X-ray diffraction (XRD) was used with equipment from Rigaku in Tokyo, Japan, to ascertain the phases, particle sizes, and crystallinity of the produced powder samples. Using a CuK source ($\lambda = 1.54178$ Å) rotating at 6°/min, an accelerating voltage of 40 kV, and a current of 40 mA, the samples were examined throughout the 20° to 85° range.

Results and Discussion

To ascertain the shape, size, distribution, surface morphology, and surface area of nanoparticles, they are subjected to various characterization methods. The characterization of any nanoparticles using XRD, SEM, and UV-Vis was utilized for each synthesized sample. The results were evident in the visual observation of the TiO_2 NP laser ablation sample; there was a noticeable change in color. As shown in Fig. 3, the color of the TiO_2-suspended solution changed from white to gray after laser irradiation for 30 minutes. After the laser irradiation, the TiO_2 powder was

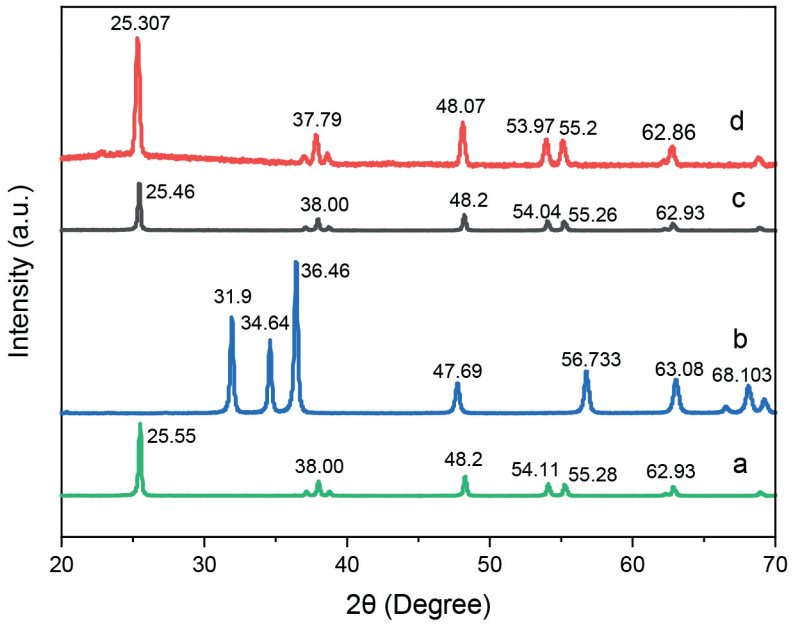

Fig. 4. XRD diffractogram of (a) raw TiO_2; TiO_2 nanoparticles prepared by: (b) ball milling (c) sonication method and (d) Laser showing the corresponding peaks.

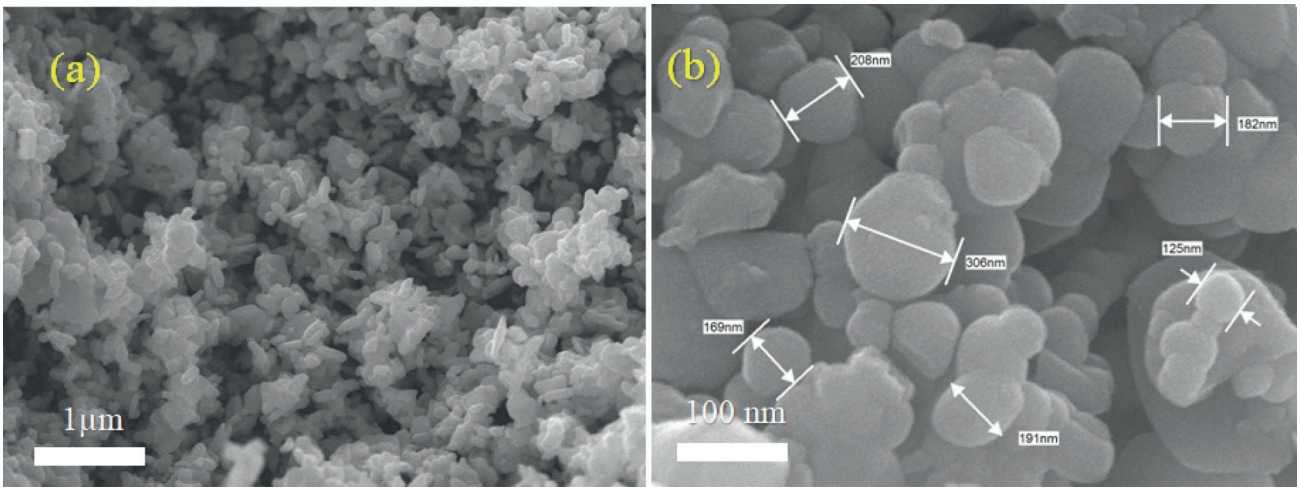

Fig. 5. SEM image of raw TiO_2 before modification at different magnifications (a) 1μm and (b) 100 nm.

dried. The characterization of samples, such as the structure of the TiO_2 before being synthesized and after being laser modified, milled, and sonicated, was explored by XRD. The powder XRD patterns of TiO_2 synthesized by different methods are shown in Fig. 4. The XRD of the processed powders illustrates the indexed and assigned peaks for the samples with similar patterns composed of peaks for bulk (raw), laser, and sonicated around 25.3°, 36.9°, 37.8°, 38.6°, 48.1°, 53.8°, and 55.2°. Different peaks were found for the milled sample at 31.9°, 34.64°, 36.46°, 47.69°, 56.73°, 63.08°, and 68.10°. The surface morphology and topology of bulk, milled, laser, and sonication samples obtained were investigated to determine the effects of each method on the morphology of TiO_2NPs, as shown in Figs. 5 and 6 (a–f). From the images presented, ball-milled for 10 h possessed an ordered, definite, and more developed porosity in comparison to pristine and other methods. Besides the significant size reduction, ball milling was observed to influence the morphology and shape of particles. The irregular shaped particles of pristine were transformed to a spherical shape on milling and then in a laser sample, but that was not clear in the sonication sample. The laser sample showed a smaller spherical shape than the milled. All samples exhibited a granular and irregular structure synonymous with the predominantly amorphous phase, as discovered in the XRD result.

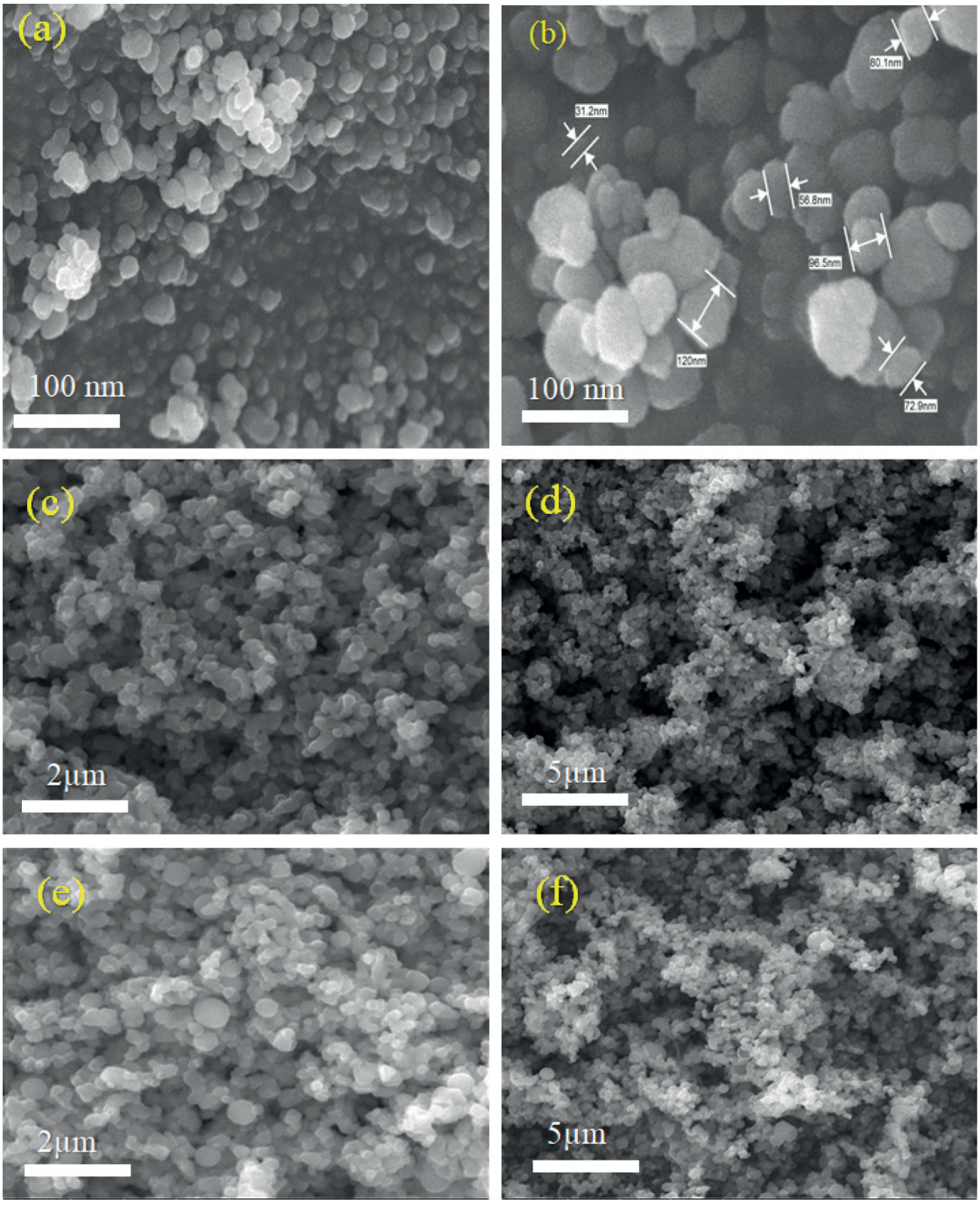

Fig. 6. SEM images of TiO_2 nanoparticles prepared by: (a), (b) ball milling; (c), (d) sonication; (e), (f) Laser method.

The image of SEM represented the spherical shape of titanium nanoparticles, with a scanning resolution speed of 1.0 nm at 5 kV with low (30,000) and high magnification (50,000). Fig. 6 represents the SEM images of the TiO_2 NPs that were prepared by different methods. The results of SEM showed that the TiO_2 nanospheres are produced, obviously, by the milling of TiO_2 nanoparticles and then in the laser sample. It could be seen that TiO_2 nanospheres appeared after laser irradiation for only 5 minutes, which increased with time. The sonication was systematically

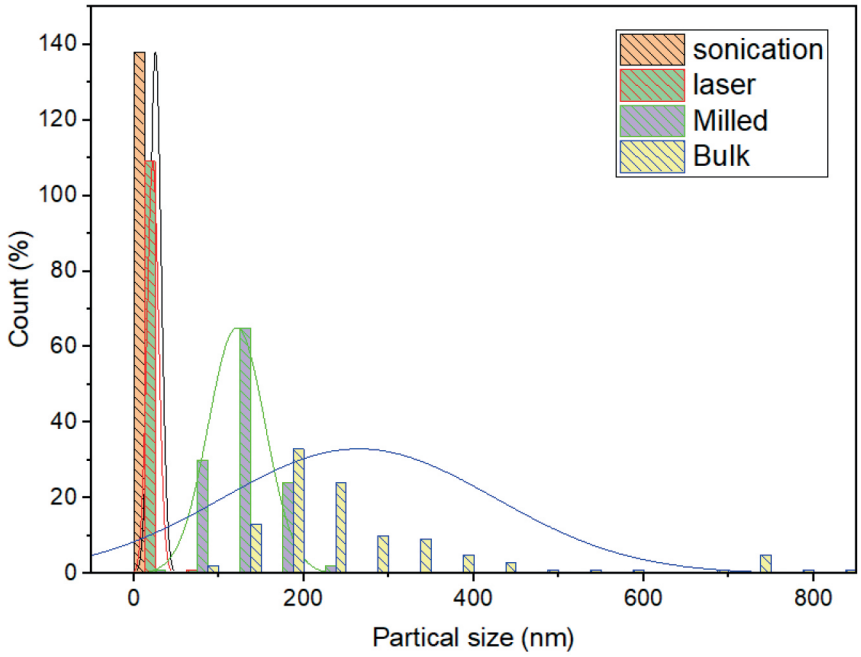

Fig. 7. Size histogram of TiO_2 nanoparticles prepared by different methods.

reduced to smaller as a function of sonication time in the 5 h range. Small particles and fragments in the micro/submicro range can be seen, and obtaining reduced-size particles by just sonication is a remarkable result. Fig. 7 shows the size histogram of TiO_2 nanoparticles prepared by sonication and laser methods. From the obtained data, the estimated diameter of each individual particle was in the range of 22.20±10.87 nm for the laser and around 25.72±8.23 nm for the sonicated sample, while the mean size for the milled sample is 196.82 nm. The SEM analysis agreed and was consistent with the above XRD data. The average crystallite size was calculated using Debye Scherrer's equation according to Oskam et al. (2003) [24]. The average was calculated at 32.9 nm, 24.86 nm, 34.42 nm, and 33.502 nm for bulk, milled, laser, and sonication, respectively. Our results were in line with Hanafy et al. (2020) [25] at pH 9 (alkaline conditions), where basic TiO_2 NPs exhibited the smallest size and were composed of only one crystalline phase (anatase phase).

The TiO_2 NPs particles sonicated for 5 h became ultrafine particles with a high porosity. The modified surface/morphology of the particles might be utilized for various applications. Lei et al. (2008) [26] reported that the application of TiO_2 NPs improved rubisco and antioxidant enzyme activities, photosynthetic rate, and chlorophyll formation, which subsequently caused enhanced crop yield. Latef et al. (2018) [27] reported a positive effect of TiO_2 NPs on the enhancement of plant growth, antioxidant enzyme activities, soluble sugars, amino acids, and proline content, in addition to a reduction in H_2O_2 and MDA contents in broad bean plants under saline conditions. Khan et. al. (2016) [28] reported mitigation of salt stress by TiO_2 NP application in tomatoes by improving agronomic traits, leaf chlorophyll content, phenolics and antioxidant capacity, antioxidant enzyme activities, and yield. TiO_2 could be considered a stimulant for plants that activates different defense mechanisms involved in plant tolerance against various abiotic stress factors [26]. These effects might vary under different environmental conditions or in diverse plant species, and based on the applied concentrations [29, 30].

Optical Properties of TiO_2 Nanoparticles

In order to carry out a more complete characterization of light absorption, several UV–Vis diffuse reflectance spectra of raw and laser irradiation TiO_2 were performed. The results are shown in Fig. 8. A sharp peak was detected in the spectrum at 390 nm, which was due to the different methods used. No other peak was observed in the spectrum, which corroborated that the TiO_2NPs possess excellent optical properties. Moreover, an enhanced absorption for photon energy has been observed in our UV-visible spectra for laser samples more than in sonication samples. It was reported that a high concentration of oxygen vacancy could break the selection rule for indirect transitions of TiO_2 and enhance absorption for photon energy below the direct band gap [31]. Furthermore, Ti^{3+} and oxygen vacancy could be induced in TiO_2 by high-energy particle bombardment [32]. In our case, it is probably due to laser irradiation that the high concentration of Ti^{3+} and oxygen vacancy are generated on the surface of TiO_2, resulting in enhanced absorption of photon energy below the direct band gap.

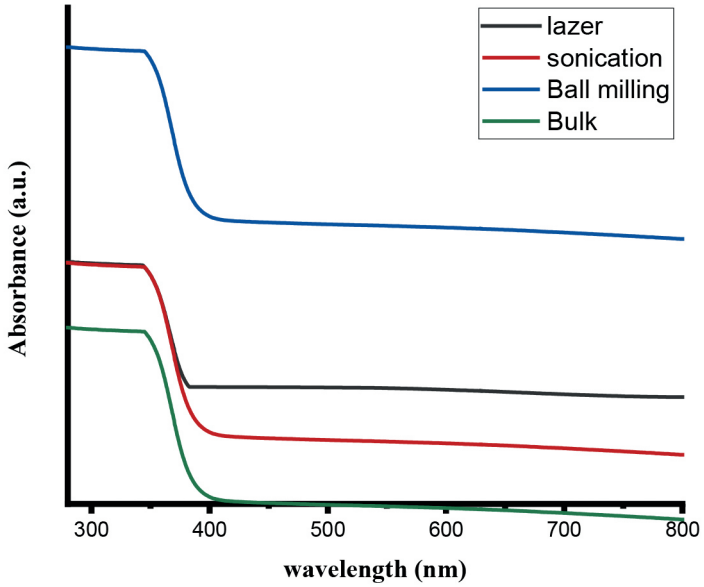

Fig. 8. The UV– visible spectrum of TiO_2NPs prepared by different methods.

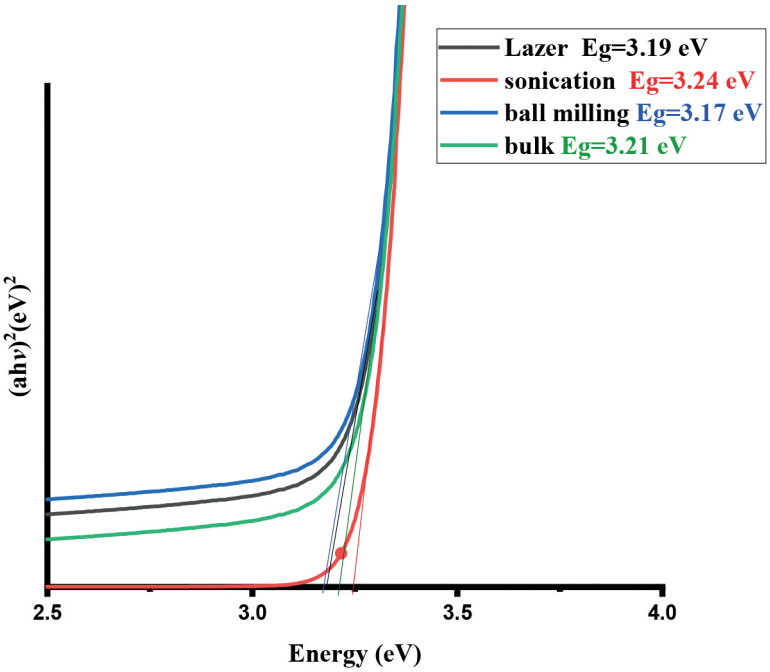

Fig. 9. Band gap energy curves of TiO_2 NPs prepared by different methods.

Experimental Test-Study the Effect of TiO_2 Preparation Methods on the Photodegradation of MB

All samples' photocatalytic activity has been assessed for the photo-degradation of methylene blue (MB), an example of organic contaminants, when confronted with visible light. In a typical photocatalytic experiment, 30 mL of a 20 parts per million water-based solution of the pollutant (MB) was ultrasonically suspended over 30 mg of TiO_2 NPs catalyst. Before being exposed to light, the mixture was shaken vigorously for thirty minutes in darkness to attain adsorption equilibrium. A visible lamp (HQI-E 400 W/n) with a maximum emission at 520 nm was next employed, and a UV filter was installed. To rule out adsorption in the dark, the substrate concentration upon equilibration was determined and designated as the equilibrium concentration (Ce). Centrifugation was used to remove the catalyst from the liquid phase after samples were taken out of the upper reactor section at various

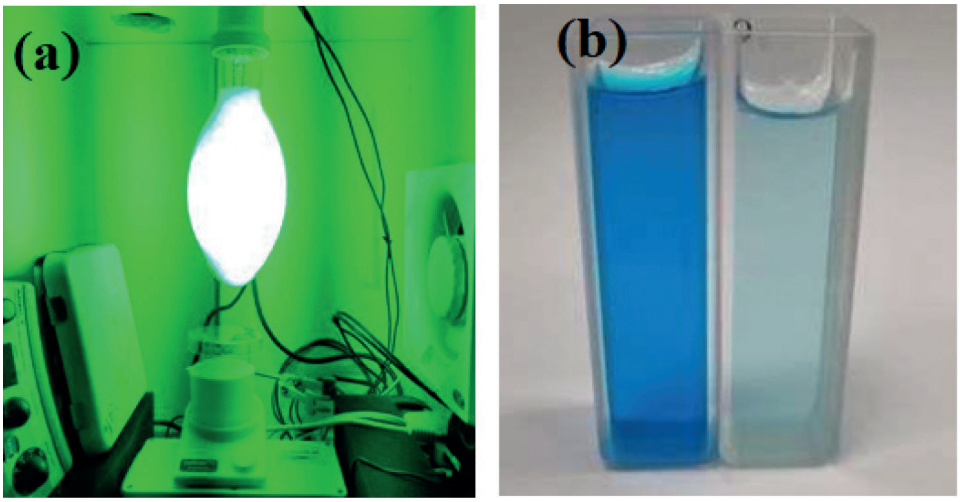

Fig. 10. (a) Experimental set-up of visible light photoreactor, (b) Methylene blue before and after 3 h of photoirradiation.

Table 1. The kinetic parameters of the photocatalytic activity of TiO_2were prepared by different mechanical methods.

Catalyst	Dark			Light	
	K_2	R^2	Qe (mg/l)	K_1	R^2
Bulk	0.00536	0.99	1.70	0.0035	0.987
Ultrasonication	0.01039	0.99	1.67	0.0049	0.999
Laser	0.05346	0.99	2.60	0.0024	0.995
Ball milling	0.00416	1	3.04	0.0033	0.999
Ball milling (cont.)	0.08354	0.94	1.35	0.0049	0.999

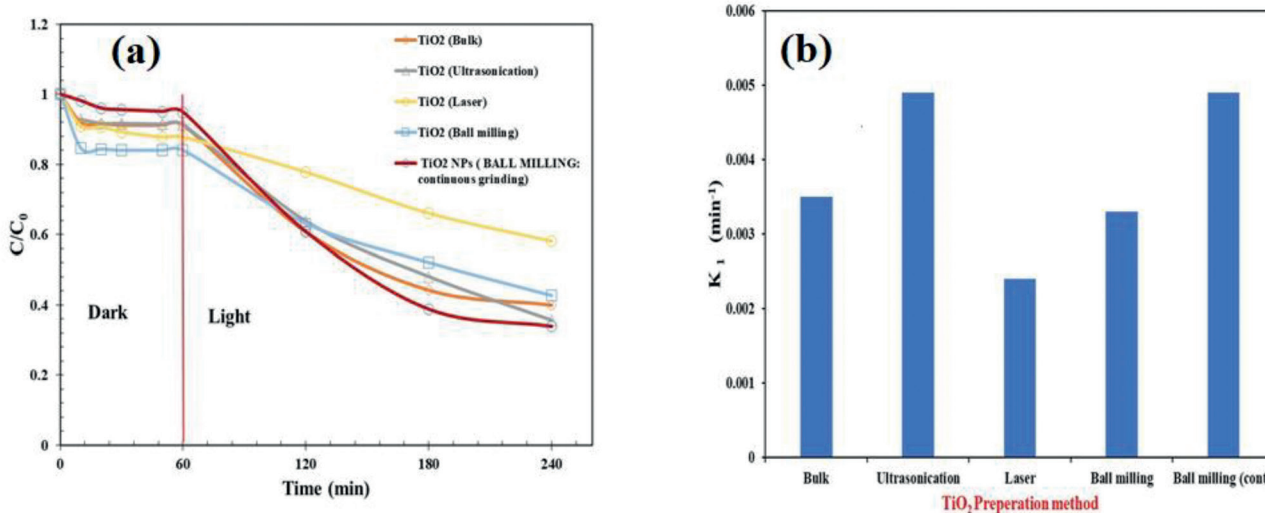

Fig. 11. Effect of the TiO_2 preparation method on degradation efficiencies of MB under UV-visible light illumination, (b) the rate constant, pseudo-first order of the TiO_2 prepared by various methods during MB degradation.

intervals (Ct). UV–Vis measurements at l = 664.47 nm using a spectrophotometer are used to calculate the dye concentration (Ct). Fig. 10 shows the dye photodegradation configuration.

The kinetics parameters were evaluated, and the constant rate of prepared samples before and after UV-visible light irradiation is shown in Table 1.

The MB degradation efficiency (DE%) was evaluated using [33]:

$$DE\% = (C_0 - C_e)/C_e \times 100$$

Where C_0 and C_e are the initial concentrations and the concentration at equilibrium of MB, respectively.

Fig. 10 (a) shows the photocatalytic activity under UV-visible light irradiation for MB degradation after 3 h of illumination. All samples demonstrated pseudo-first order, and the photocatalytic performance was sorted as follows: TiO_2 Ultrasonication / TiO_2 Ball Milling (cont.) > TiO_2 Bulk > TiO_2 Ball Milling > TiO_2 Laser. Fig. 10(b). The highest degradation rate ($K = 0.0049\ min^{-1}$) was observed for TiO_2 produced through continuous balling and ultrasonication, which was probably caused by the decrease in particle size as discussed in the SEM section. The size of the particle influences the photocatalytic efficiency since the smallest particles have more surface areas and a greater number of photoactive sites per unit area. It has been found that ball milling conditions affect the photoperformance of TiO_2 nanoparticles, as reported by Saitow et al. [34]. Their results demonstrated that TiO_2 photocatalytic activity increases by 63-fold after milling due to particle size reduction. In another study, Tiple et.al. [35] found similar results when ultrasonicating TiO_2 to desulfurize thiophene. The particle size was reduced linearly with ultrasonication power and time (Fig. 11).

Conclusions

The study utilized three straightforward, cost-effective, and environmentally friendly synthesis methods – ball milling, laser irradiation, and sonication – to produce three distinct types of TiO_2 nanoparticles. These methods demonstrated their efficacy in manipulating the physical characteristics of the nanoparticles, specifically their size, which is important for various applications. Detailed observations from the study indicated that the preparation process significantly influenced the TiO_2 particle size. Specifically, the crystallite sizes were measured to be approximately 24.86 nm, 33.5 nm, and 34.4 nm for high-energy ball milling, sonication, and pulse laser ablation methods, respectively. Furthermore, the average particle sizes were noted as 121.2 nm, 25.53 nm, and 22.38 nm for each respective method. Among the methods, ultrasonication and continuous ball milling were particularly noteworthy, as they exhibited superior performance in enhancing the TiO_2 photocatalytic activity. The findings of this study not only contribute to the understanding of nanoparticle synthesis but also underscore the potential of simple, yet effective, modifications in the synthesis process to significantly improve the performance of photocatalytic devices. The implications of this research are far-reaching, offering a promising outlook for the development of more efficient and effective photocatalytic devices, thereby advancing the field and paving the way for future innovations.

Acknowledgements

The authors would like to thank the Deanship of Scientific Research at Umm Al-Qura University for supporting this work by Grant Code: (22UQU4280488DSR02).

Conflict of Interest

The authors declared no conflict of interest among them.

References

1. PATNAIK J.N., SAHU A.K., POONIA P., GHOSH, P. Current perspective of nano-engineered metal oxide based photocatalysts in advanced oxidation processes for degradation of organic pollutants in wastewater. Polish Journal of Environmental Studies, 22 (**4**), 667, **2023**.
2. YE T., LIU L., WANG Y., ZHANG J., WANG C., LI L. Efficient Degradation of Rhodamine B Dye through Hand Warmer Heterogeneous Activation of Persulfate. Sustainability, 15, 13034, **2023**.
3. NAVIDPOUR A.H., ABBASI S., LI D., MOJIRI A., ZHOU J.L. Investigation of Advanced Oxidation Process in the Presence of TiO2 Semiconductor as Photocatalyst: Property, Principle, Kinetic Analysis, and Photocatalytic Activity. Catalysts, **13**, 232, **2023**.
4. BENČINA M., IGLIČ A., MOZETIČ M., JUNKAR I. Crystallized TiO_2 Nanosurfaces in Biomedical Applications. Nanomaterials, 10, 1121, **2023**.
5. EDDY D.R., PERMANA M.D., SAKTI L.K., SHEHA G.A., SOLIHUDIN, HIDAYAT S., TAKEI T., KUMADA N., RAHAYU I. Heterophase Polymorph of TiO_2 (Anatase, Rutile, Brookite, TiO_2 (B)) for Efficient Photocatalyst: Fabrication and Activity. Nanomaterials, 13 (**4**), 704, **2023**.
6. CATAURO M., TRANQUILLO E., DAL POGGETTO G., PASQUALI M., DELL'ERA A., VECCHIO CIPRIOTI S. Influence of the heat treatment on the particles size and on the crystalline phase of TiO2 synthesized by the sol-gel method. Materials, 11, 2364, **2018**.
7. PAYORMHORM J., IDEM R. Synthesis of C-doped TiO2 by sol-microwave method for photocatalytic conversion of glycerol to value-added chemicals under visible light. Applied Catalysis A: General, 590, 117362, **2020**.
8. NAGARAJ G., RAJ A.D., IRUDAYARAJ A.A., JOSEPHINE R.L. Tuning the optical band Gap of pure TiO2 via photon induced method. Optik, 179, 889, **2018**.
9. WANG J., WANG Z., WANG W., WANG Y., HU X., LIU J., GONG X., MIAO W., DING L., LI X., TANG J. Synthesis, modification and application of titanium dioxide nanoparticles: a review. Nanoscale, **14** (18), **2022**.
10. HU J., ZHANG S., CAO Y., WANG H., YU H., PENG F. Novel highly active anatase/rutile TiO_2 photocatalyst with hydrogenated heterophase interface structures for photoelectrochemical water splitting into hydrogen. ACS Sustainable Chemistry & Engineering, 6 (**8**), 10823, **2018**.
11. JIMENEZ-RELINQUE E., CASTELLOTE M. Hydroxyl radical and free and shallowly trapped electron generation and electron/hole recombination rates in TiO2 photocatalysis using different combinations of anatase and rutile. Applied Catalysis A: General, 565, 20, **2018**.
12. HOFFMANN M., MARTIN S., CHOI W., BAHNEMANN D. Photocatalysis on TiO2 surfaces-principles, mechanisms, and selected results. Chemical Reviews, 95, 69, **1995**.
13. AHMAD M.M., MUSHTAQ S., AL QAHTANI H.S., SEDKY A., ALAM M.W. Investigation of TiO_2 Nanoparticles Synthesized by Sol-Gel Method for Effectual Photodegradation, Oxidation and Reduction Reaction. Crystals, 11 (**12**), 1456, **2021**.
14. DUDINA D.V., BOKHONOV B.B. Materials development using high-energy ball milling: A review dedicated to the memory of MA Korchagin. Journal of Composites Science, **6** (7), 188, **2022**.
15. ARZT E., SCHULTZ L. New materials by mechanical alloying techniques. Material and Manufacturing Process, **6** (4),733, **1991**.

16. RANE A.V., KANNY K., ABITHA V.K., THOMAS S. Methods for synthesis of nanoparticles and fabrication of nanocomposites. In Synthesis of Inorganic Nanomaterials. Woodhead Publishing, 121, **2018**.
17. RAJPUT N. Methods of preparation of nanoparticles-a review. International Journal of Advances in Engineering & Technology, **7** (6), 1806, **2015**.
18. AL BAROOT A., HALADU S.A., IBRAHIM M.B., AKHTAR S., ALSHAMMARI A.H., TAHA T.A., MANDA A.A. Enhancement of catalytic reduction of 4-nitrophenol using MoO3 nanobelts incorporated SiO2 nanocomposite fabricated by nanosecond pulsed laser ablation technique. Physica Scripta, **98** (9), 095002, **2023**.
19. GHORBANI H.R. A review of methods for synthesis of Al nanoparticles. Oriental Journal of Chemistry, **30** (4), 1941, **2014**.
20. JAMKHANDE P.G., GHULE N.W., BAMER A.H., KALASKAR M.G. Metal nanoparticles synthesis: An overview on methods of preparation, advantages and disadvantages, and applications. Journal of Drug Delivery Science and Technology, **53**, 101174, **2019**.
21. MANSOUREH G., PARISA V. Synthesis of metal nanoparticles using laser ablation technique. In Emerging Applications of Nanoparticles and Architecture Nanostructures. Elsevier, 575, **2018**.
22. SIMAKIN A.V., VORONOV V.V., KIRICHENKO N.A., SHAFEEV G.A. Nanoparticles are produced by laser ablation of solids in liquid environment. Applied Physics A: Materials Science & Processing, **79**, 1127, **2004**.
23. CHOU K.S., LAI Y.S. Effect of polyvinyl pyrrlidone molecular weights on the formation. Materials Chemistry and Physics, **83** (1), 82, **2004**.
24. OSKAM G., NELLORE A., LEE PENN R., SEARSON P.C. The growth kinetics of TiO_2 nanoparticles from titanium (IV) alkoxide at high water/titanium ratio. Journal of Physical Chemistry B, **107** (8), 1734, **2003**.
25. HANAFY M.S., ABDEL FADEEL D.A., ELYWA M.A., KELANY N.A. Green synthesis and characterization of TiO_2 nanoparticles Using (*Aloe vera*) Extract at Different pH Value. Science Journal of King Faisal University/Basic and Applied Sciences, **21** (1), 103, **2020**.
26. LEI Z., MINGYU S., XIAO W., CHAO L., CHUNXIANG Q., LIANG C., FASHUI H. Antioxidant stress is promoted by nano-anatase in spinach chloroplasts under UV-B radiation. Biological Trace Element Research, **121**, 69, **2008**.
27. ABDEL LATEF A.A.H., SRIVASTAVA A.K., EL-SADEK M.S.A., KORDROSTAMI M., TRAN L.S.P. Titanium dioxide nanoparticles improve growth and enhance tolerance of broad bean plants under saline soil conditions. Land Degradation & Development, **29** (4), 1065, **2018**.
28. KHAN M.N. Nano-titanium dioxide (nano-TiO_2) mitigates NaCl stress by enhancing antioxidative enzymes and accumulation of compatible solutes in tomato (*Lycopersicon esculentum* Mill.). Journal of Plant Sciences, **11** (1), 1, **2016**.
29. FEIZI H., REZVANI MOGHADDAM P., SHAHTAHMASSEBI N., FOTOVAT A. Impact of bulk and nanosized titanium dioxide (TiO_2) on wheat seed germination and seedling growth. Biological Trace Element Research, **146**, 101, **2012**.
30. TAN W., PERALTA-VIDEA J.R., GARDEA-TORRESDEY J.L. Interaction of titanium dioxide nanoparticles with soil components and plants: current knowledge and future research needs–a critical review. Environmental Science: Nano, **5** (2), 257, **2018**.
31. ZUO F., WANG L., WU T., ZHANG Z.Y., BORCHARDT D., FENG P.Y. Self-Doped Ti^{3+} Enhanced Photocatalyst for Hydrogen Production under Visible Light. Journal of the American Chemical Society, **132** (34), 11856, **2010**.
32. THOMPSON T.L., YATES J.T. Surface Science Studies of the Photoactivation of TiO2-New Photochemical Processes. Chemical Reviews, **106** (10), 4428, **2006**.
33. GUARALDO T.T., PULCINELLI S.H., ZANONI M.V.B. Influence of particle size on the photoactivity of Ti/TiO_2 thin film electrodes, and enhanced photoelectrocatalytic degradation of indigo carmine dye. Journal of Photochemistry and Photobiology A: Chemistry, **217** (1), 259, **2011**.
34. SAITOW K.I., WAKAMIYA T. 130-fold enhancement of TiO_2 photocatalytic activities by ball milling. Applied Physics Letters, **103** (3), 031916, **2013**.
35. TIPLE A., SINHMAR P.S., GOGATE P.R. Improved direct synthesis of TiO_2 catalyst using sonication and its application for the desulfurization of thiophene. Ultrasonics Sonochemistry, **3**, 105547, **2021**.